Full Paper

Propellants, Explosives, Pyrotechnics

DOI: 10.1002/prep.201400244

A 3D Smoothed Particle Hydrodynamics Method with Reactive Flow Model for the Simulation of ANFO

Guangyu Wang,*[a] Guirong Liu,[a] Qing Peng,[b] Suvranu De,[b] Dianlei Feng,[c] and Moubin Liu[c]

Abstract: ANFO (ammonium nitrate/fuel oil) is a widely used bulk industrial explosive mixture that is considered to be highly "non-ideal" with long reaction zones, low detonation energies, and large failure diameters. Thus, its detonation poses great challenge for accurate numerical modeling. Herein, we present a numerical model to simulate ANFO based on improved smoothed particle hydrodynamics (SPH) method, which is a mesh-free Lagrangian method performing well in simulating situations consist of moving interface and large deformation, as happened in high-velocity impact and explosion. The improved three-dimensional SPH method incorporated with JWL++ model is used to simulate the detonation of ANFO. Good agreement is observed between simulation and experiment, which indicates that the proposed method performs well in prediction of behavior of ANFO.

Keywords: ANFO · Smoothed particle hydrodynamics (SPH) · Size effect · Detonation · Numerical simulation

1 Introduction

ANFO is an explosive mixture of ammonium nitrate (AN, 94 wt-%) and fuel oil (FO, 6 wt-%) with a density of 800 to 1000 kg m^{-3}. It is known as highly non-ideal, high-porosity and low-density explosive, where the fuel and oxidizer are not mixed at the molecular level [1,2]. Differing from other explosives such as TNT, it exhibits special characteristics such as low detonation velocity, long reaction zones, low detonation energies, and large failure diameters.

The characteristics of ANFO have been studied a lot by many researchers through experiments [3,4] and theoretical studies [5]. Catanach, Hill, and Davis conducted series of experiments on diameter effect of ANFO, and measured the curvature of detonation front using ANFO cylinders [3,4]. Bdzil and Aslam proposed Detonation Shock Dynamics (DSD) theory that the velocity of detonation normal to the shock is solely a function of the shock curvature, and incorporated the model in their code [5]. For the numerical modelling of non-ideal explosives, Borg and Jones investigated projectile impact experiments using a fire reaction rate model [6]. Kapila, Schwendeman, and Bdzil described the Ignition-and-Growth model in a finite-volume method and applied the model in simulation of LX-17 [7,8]. Souers described a simplified reactive flow model (JWL++ model) and applied the model in the study of size effect of ANFO K1 [9]. Tarver and McGuire applied Ignition-and-Growth model in the investigation of detonation waves of confined high explosive LX-17, PBX 9502, and EDC-35 [10]. Garcia and Tarver further described a 3D Ignition-and-Growth reactive flow model of PBX 9502 and compared simulation with experiment [11]. Guilkey, Harman et al. described a 3D Eulerian-Lagrangian approach and applied it in the simulation of size effect and copper-confined explosion of ANFO [12]. Kim and Yoh [13] investigated size effect and copper-confined ANFO using an Eulerian method. Besides these continuum models for the mixtures, the pure ammonium nitrate is also an interest in atomistic-level studies, including mechanical properties [14] and equations of state [15,16].

The SPH method was first proposed by Gingold, Monaghan, and Lucy [17,18] to study astrophysics. Afterwards, due to the advantages of SPH method in tracking moving interfaces and dealing with large deformation, it has been applied to solve fluid dynamic problems and beyond, explosion, and hypervelocity impact problems. Liu, Liu et al. [19–23] investigated the feasibility of using SPH to simulate explosion of high explosive, underwater explosion, shaped charge detonation, and so on. In this paper, the SPH method has been applied in the simulation of detonation of 3D ANFO cylinders, where heterogeneous materials and their interaction, phase transformation, large deformation

[a] G. Wang, G. Liu
School of Aerospace Systems
University of Cincinnati
Cincinnati, OH 45221-0070, USA
*e-mail: wangg3@mail.uc.edu

[b] Q. Peng, S. De
Department of Mechanical, Aerospace and Nuclear Engineering
Rensselaer Polytechnic Institute
Troy, NY 12180, USA

[c] D. Feng, M. Liu
Key Laboratory for Mechanics in Fluid-Solid Coupling Systems
Institute of Mechanics
Chinese Academy of Sciences
Beijing, 100190, P. R. China

and high strain rate are involved, to which the SPH method can be of advantageous.

In this paper, an improved SPH method incorporated with JWL++ model is proposed to simulate detonation of series of ANFO cylinders. Then, the simulation is compared with experiment and good agreement is observed, which indicates that the proposed method can well predict the behavior of ANFO in detonation.

2 Theoretical Formulation of SPH

2.1 Function Approximation in SPH

SPH was formulated to solve hydrodynamics problems that are governed in form of partial differential equations (PDEs) with primary field variables of density, velocity, and energy [19]. It was also extended to solve problems such as solid mechanics [18]. In SPH method, the entire domain is discredited by a finite number of particles that carry individual mass and occupy individual space. Any field function $f(\boldsymbol{x})$ in the problem domain can be approximated in SPH as follow [19]:

$$\langle f(\boldsymbol{x})\rangle = \int_{\Omega} f(\boldsymbol{x}')W(\boldsymbol{x}-\boldsymbol{x}',h)\mathrm{d}\boldsymbol{x}' \tag{1}$$

where Ω is the problem domain, f is a field function related to the three-dimensional position vector $\boldsymbol{x}$, $W(\boldsymbol{x}-\boldsymbol{x}', h)$ is the smoothing kernel function. h is the smoothing length, which defines the influence area of the smoothing function W.

The smoothing function W should be chosen to satisfy a number of conditions. The first is called the normalization condition:

$$\int_{\Omega} W(\boldsymbol{x}-\boldsymbol{x}',h)\mathrm{d}\boldsymbol{x}' = 1 \tag{2}$$

The second is called the Delta function property:

$$\lim_{h\to 0} W(\boldsymbol{x}-\boldsymbol{x}',h) = \delta(\boldsymbol{x}-\boldsymbol{x}') \tag{3}$$

The latter is called the compact condition:

$$W(\boldsymbol{x}-\boldsymbol{x}',h) = 0 \text{ when } |\boldsymbol{x}-\boldsymbol{x}'| > \kappa h \tag{4}$$

where κ is a scalar factor associated with the smoothing function for point at $\boldsymbol{x}$. It defines the effective area of the smoothing function. The effective area is called support domain for the point at $\boldsymbol{x}$.

Based on the product rule for derivatives and the Gaussian Law, the derivative of function $f(\boldsymbol{x})$ can be derived as follow:

$$\langle \nabla\cdot f(\boldsymbol{x})\rangle = \int_{S} f(\boldsymbol{x}')W(\boldsymbol{x}-\boldsymbol{x}',h)\cdot\vec{\boldsymbol{n}}dS - \int_{\Omega} f(\boldsymbol{x})\cdot\nabla W(\boldsymbol{x}-\boldsymbol{x}',h)\mathrm{d}\boldsymbol{x}' \tag{5}$$

where $\vec{n}$ is the unit vector normal to the surface S. If the support zone is within problem domain, according to compact condition of smoothing kernel function, we have:

$$W(\boldsymbol{x}-\boldsymbol{x}',h) = 0 \tag{6}$$

Therefore,

$$f(\boldsymbol{x}')W(\boldsymbol{x}-\boldsymbol{x}',h) = 0 \tag{7}$$

Thus, Equation (5) can be rewritten as:

$$\langle \nabla\cdot f(\boldsymbol{x})\rangle = -\int_{\Omega} f(\boldsymbol{x})\cdot\nabla W(\boldsymbol{x}-\boldsymbol{x}',h)\mathrm{d}\boldsymbol{x}' \tag{8}$$

To calculate the integration of Equation (1) and Equation (5), a summation over all particles within the support domain is implemented, as shown in Figure 1.

Therefore, Equation (1) and Equation (8) can be rewritten as:

$$\langle f(\boldsymbol{x}_i)\rangle = \sum_{j=1}^{N}\frac{m_j}{\rho_j}f(\boldsymbol{x}_j)W_{ij} \tag{9}$$

$$\langle \nabla\cdot f(\boldsymbol{x}_i)\rangle = -\sum_{j=1}^{N}\frac{m_j}{\rho_j}f(\boldsymbol{x}_j)\cdot\nabla W_{ij} \tag{10}$$

where

$$W_{ij} = W(\boldsymbol{x}_i-\boldsymbol{x}_j,h) \tag{11}$$

2.2 Discretization of Governing Equations

The governing equations for hydrodynamics problems are Navier-Stokes equations. The standard Lagrangian form of the Navier-Stokes equations consists of, first, the continuity Equation [19]:

$$\frac{\mathrm{d}\rho}{\mathrm{d}t} = -\rho\frac{\partial \boldsymbol{v}^{\beta}}{\partial \boldsymbol{x}^{\beta}} \tag{12}$$

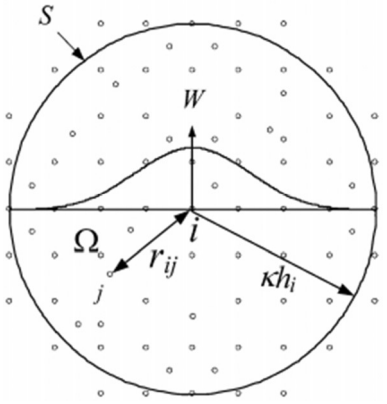

Figure 1. Support zone of particle *i*.

Second, the momentum equation:

$$\frac{\mathrm{d}\boldsymbol{v}^{\alpha}}{\mathrm{d}t}=\frac{1}{\rho}\frac{\partial\sigma^{\alpha\beta}}{\partial\boldsymbol{x}^{\beta}} \tag{13}$$

Third, the energy equation:

$$\frac{\mathrm{d}e}{\mathrm{d}t}=\frac{\sigma^{\alpha\beta}}{\rho}\frac{\partial\boldsymbol{v}^{\alpha}}{\partial\boldsymbol{x}^{\beta}} \tag{14}$$

where ρ is the density, e is the internal energy, v^{α} is the velocity, and $\sigma^{\alpha,\beta}$ is the total stress tensor, which are all dependent variables. $\boldsymbol{x}^{\alpha}$ is the spatial coordinate and t is the time, which are both independent variables. The total stress tensor $\sigma^{\alpha,\beta}$ consists of two parts, one is the isotropic pressure p and the other is shear stress $\tau^{\alpha,\beta}$:

$$\sigma^{\alpha\beta}=-p\delta^{\alpha\beta}+\tau^{\alpha\beta} \tag{15}$$

For the explosive gas, the viscous shear stress can be neglected compared with the isotropic pressure. For solid materials, shear stress can be obtained from constitutive equations of material.

By implementing the SPH method to approximate density of particle, an approach called continuity density is employed. After manipulation, Equation (12) can be rewritten as:

$$\frac{\mathrm{d}\rho}{\mathrm{d}t}=-\rho_i\sum_{j=1}^{N}\frac{m_j}{\rho_j}\boldsymbol{v}_j^{\beta}\frac{\partial W_{ij}}{\partial\boldsymbol{x}_i^{\beta}} \tag{16}$$

Similarly, Equation (13) and Equation (14) can be rewritten as follows:

$$\frac{\mathrm{d}\boldsymbol{v}_i^{\alpha}}{\mathrm{d}t}=-\sum_{j=1}^{N}m_j\left(\frac{\sigma_i^{\alpha\beta}}{\rho_i^2}+\frac{\sigma_j^{\alpha\beta}}{\rho_j^2}+\Pi_{ij}\right)\frac{\partial W_{ij}}{\partial\boldsymbol{x}_i^{\beta}} \tag{17}$$

$$\frac{\mathrm{d}e_i}{\mathrm{d}t}=\frac{1}{2}\sum_{j=1}^{N}m_j\left(\frac{p_i}{\rho_i^2}+\frac{p_j}{\rho_j^2}+\Pi_{ij}\right)\left(\boldsymbol{v}_i^{\beta}-\boldsymbol{v}_j^{\beta}\right)\frac{\partial W_{ij}}{\partial\boldsymbol{x}_i^{\beta}}+\frac{1}{\rho_i}S_i^{\alpha\beta}\varepsilon_i^{\alpha\beta} \tag{18}$$

where $\varepsilon^{\alpha,\beta}$ is the strain rate tensor and Π is the artificial viscosity.

2.3 Artificial Viscosity

In order to simulate the transformation of kinetic energy to heat energy across the shock wave front, Monaghan type artificial viscosity Π_{ij} is introduced in the implementation of SPH [19, 24–26], which can be written as:

$$\Pi_{ij}=\begin{cases}\dfrac{-\alpha\overline{c}_{ij}\phi_{ij}+\beta\phi_{ij}^2}{\overline{\rho}_{ij}} & ,\quad \boldsymbol{v}_{ij}\cdot\boldsymbol{x}_{ij}<0\\ 0 & ,\quad \boldsymbol{v}_{ij}\cdot\boldsymbol{x}_{ij}\geq 0\end{cases} \tag{19}$$

where

$$\phi_{ij}=\frac{h_{ij}\boldsymbol{v}_{ij}\boldsymbol{x}_{ij}}{\left|\boldsymbol{x}_{ij}\right|^2+\varphi^2} \tag{20}$$

$$\overline{c}_{ij}=\frac{1}{2}(c_i+c_j) \tag{21}$$

$$\overline{\rho}_{ij}=\frac{1}{2}(\rho_i+\rho_j) \tag{22}$$

$$h_{ij}=\frac{1}{2}(h_i+h_j) \tag{23}$$

$$\boldsymbol{v}_{ij}=\boldsymbol{v}_i-\boldsymbol{v}_j \tag{24}$$

$$\boldsymbol{x}_{ij}=\boldsymbol{x}_i-\boldsymbol{x}_j \tag{25}$$

where α and β are constants. ϕ is used to prevent numerical divergences between two particles, c and $\boldsymbol{v}$ represent the speed of sound and velocity of particle, respectively. The viscosity term associated with α produces a bulk viscosity, while the second term associated with β is intended to suppress particle interpenetration at high Mach number. α, β, ϕ is set to be 1, 1, and 0.1, respectively, in all our simulation.

2.4 Kernel Gradient Correction

To reduce particle inconsistency and improve SPH approximation accuracy, a Kernel Gradient Correction (KGC) method is applied. It has been demonstrated that under circumstances such as irregular particle distribution, variable smoothing length, truncated boundary areas, the SPH method with KGC is of second-order accuracy [27].

The implementation of KGC method can be described as follow: first, a local reversible matrix $\boldsymbol{L}(\boldsymbol{r}_i)$ is calculated using Taylor series, then, the original kernel gradient is multiplied by $\boldsymbol{L}(\boldsymbol{r}_i)$ to obtain modified kernel gradient.

In the condition of three-dimensional simulation, the modified kernel gradient of smoothing function $\nabla_i^{C}V_{ij}$ can be calculated as follow:

$$\nabla_i^{C}W_{ij}=\boldsymbol{L}(\boldsymbol{r}_i)\nabla_i W_{ij} \tag{26}$$

where

$$\boldsymbol{L}(\boldsymbol{r}_i)=\left(\sum_j\begin{pmatrix}\boldsymbol{x}_{ji}\dfrac{\partial W_{ij}}{\partial x_i} & \boldsymbol{y}_{ji}\dfrac{\partial W_{ij}}{\partial x_i} & \boldsymbol{z}_{ji}\dfrac{\partial W_{ij}}{\partial x_i}\\ \boldsymbol{x}_{ji}\dfrac{\partial W_{ij}}{\partial y_i} & \boldsymbol{y}_{ji}\dfrac{\partial W_{ij}}{\partial y_i} & \boldsymbol{z}_{ji}\dfrac{\partial W_{ij}}{\partial y_i}\\ \boldsymbol{x}_{ji}\dfrac{\partial W_{ij}}{\partial z_i} & \boldsymbol{y}_{ji}\dfrac{\partial W_{ij}}{\partial z_i} & \boldsymbol{z}_{ji}\dfrac{\partial W_{ij}}{\partial z_i}\end{pmatrix}V_j\right)^{-1} \tag{27}$$

V_j is the volume of particle j. $\boldsymbol{x}_{ij}$, $\boldsymbol{y}_{ij}$, and $\boldsymbol{z}_{ij}$ is given by:

$$\boldsymbol{x}_{ji} = \boldsymbol{x}_j - \boldsymbol{x}_i \tag{28}$$

$$\boldsymbol{y}_{ji} = \boldsymbol{y}_j - \boldsymbol{y}_i \tag{29}$$

$$\boldsymbol{z}_{ji} = \boldsymbol{z}_j - \boldsymbol{z}_i \tag{30}$$

2.5 Smoothing Length Update

The following method is used to update the smoothing length of each particle during the implementation of SPH simulation [28]:

$$\frac{\mathrm{d}h_i^n}{\mathrm{d}t} = -\frac{h_i^n}{\rho_i^n d}\frac{\mathrm{d}\rho_i^n}{\mathrm{d}t} \tag{31}$$

where h_i^{n} ρ_i^{n} are smoothing length and density of particle *i* at time step *n*. For convenience, Equation (21) can be further written in the form:

$$\frac{\mathrm{d}h_i^n}{\mathrm{d}t} = -\frac{h_i^n}{\rho_i^n d}\sum_{j=1}^{N} m_j(\boldsymbol{v}_i^n - \boldsymbol{v}_j^n)\cdot\nabla_i^n W_{ij} \tag{32}$$

where $\boldsymbol{v}_i^{\mathrm{n}}$ and $\nabla_i^{\mathrm{n}} W_{ij}$ are velocity and kernel gradient of particle *i* at time step *n*.

Thus, the smoothing length at the next step becomes:

$$h_i^{n+1} = h_i^n + \frac{\mathrm{d}h_i^n}{\mathrm{d}t}\Delta t \tag{33}$$

3 Equations of State and Constitutive Modeling

3.1 JWL++ Model

The JWL++ model is incorporated with our improved SPH code to simulate ANFO. Compared with the standard Jones-Wilkins-Lee (JWL) that uses a single Equation of state (EoS), JWL++ model introduces an extra EoS for unreacted explosive. It also allows the simulation of ignition, which means that the explosive can be detonated by impact. Besides the extra EoS for unreacted explosive, JWL++ model keeps the standard JWL EoS for explosive products. The JWL EoS is an empirical mathematical expression written in terms of specific internal energy, pressure and specific volume of explosive products [29–31]. It is used to calculate the pressure of explosive products as they expand from a certain high-pressure, high-density state after detonation to terminal state at normal pressure, and gaseous density. The JWL EoS works well for ideal explosive like TNT. JWL++ model is a simplified model that includes time-dependent chemical reaction, allowing the ignition as well as the reaction process to be modeled. The JWL++ model can reproduce the size effect and detonation front curvature [9]. It mainly consists of the following parts:

First, the unreacted explosive is modelled using the Murnahan EoS:

$$p_{\mathrm{unreacted}} = \frac{1}{n\kappa}\left(\frac{1}{\upsilon^n} - 1\right) \tag{34}$$

where $p_{\mathrm{unreacted}}$ is the pressure of unreacted explosive, *n* and κ are constants determined by experiment, υ is the relative volume, which is given by

$$\upsilon = \frac{\rho_0}{\rho} \tag{35}$$

The speed of sound for the Murnahan EoS is given by:

$$c^2_{\mathrm{unreacted}} = -\frac{\upsilon^2}{\rho_0}\frac{dP_{\mathrm{unreacted}}}{d\upsilon} = \frac{1}{\rho_0\kappa\upsilon^{n-1}} \tag{36}$$

Second, the modified JWL EoS is used to describe explosive products:

$$p_{\mathrm{reacted}} = A\exp(-R_1\upsilon) + B\exp(-R_2\upsilon) + \frac{C}{\upsilon^{1+\omega}} \tag{37}$$

where *A*, *B*, *C*, R_1, R_2, ω are constants derived from experiments.

The speed of sound used in the JWL EoS is given by:

$$c^2_{\mathrm{reacted}} = -\frac{\upsilon^2}{\rho_0}\frac{dp_{\mathrm{reacted}}}{d\upsilon} = \frac{\upsilon^2}{\rho_0}\left(AR_1\exp(-R_1\upsilon) + BR_2\exp(-R_2\upsilon) + C\frac{1+\omega}{\upsilon^{2+\omega}}\right) \tag{38}$$

Third, a rule of mixture is used to combine these two EoSs for intermediate stages of ANFO:

$$p_{\mathrm{total}} = (1-F^m)p_{\mathrm{unreacted}} + F^m p_{\mathrm{reacted}} \tag{39}$$

where *F* is the burn fraction, *m* is usually 1. Similarly, the speed of sound is estimated using the same rule of mixture.

$$c^2_{\mathrm{total}} = (1-F^m)c^2_{\mathrm{unreacted}} + F^m c^2_{\mathrm{reacted}} \tag{40}$$

Finally, the reaction rate can be described using the following formula,

$$\frac{dF}{dt} = G(p+Q)^b(1-F) \tag{41}$$

where *G* is the rate constant, *b* is the power of the pressure and *Q* is the artificial viscosity, which is set to be 0 in all cases.

In the implementation of JWL++ model, the state of explosive can be described by reaction progress that is between 0 and 1. 0 represents unreacted solid explosive, 1 represents the fully reacted explosive gas, and the

Table 1. Detonation velocity of ANFO cylinders obtained from experiment [3].

Charge diameter Ø [mm]	77	90	102	115	128	153
Detonation velocity (experiment) D_0 [m s^{-1}]	1570.51	2467.95	2852.56	3108.97	3317.31	3621.79

number between 0 and 1 represents explosion products in the mixing state.

4 Numerical Examples

In this section, a 3D simulation of detonation of ANFO cylinders, which is used to reproduce size effect, is implemented using our improved SPH code, and the results are compared with experiment.

4.1 Study on Size Effect

ANSYS® is used to generate the initial particles for our SPH code. The process can be described as follow:

First, the 3D geometric domain is meshed using tetrahedron elements. Tetrahedron element is preferred because they can be automatically generated for any complex geometry. Then, at the geometric center of each tetrahedron, a particle is generated, as shown in Figure 2. The element edge length l of tetrahedron is used to control the total number of particles used in the model.

Size effect is a typical characteristic of ANFO, which refers to the phenomenon that the detonation velocity varies considerably with the diameter of ANFO cylinder. In this section, the detonation of six ANFO cylinders with diameters ranging from 77 mm to 153 mm is simulated, as listed in Table 1. The density values of all ANFO are identically set to be 880 kg m^{-3}. The length-to-diameter (LD) ratio in all cases is 10.

All cylinders are detonated by impacting from one end, as shown in Figure 3, where the v_z of red particles is set to be 500 m s^{-1}. The instant detonation velocity is calculated at each time step based on the location of detonation front.

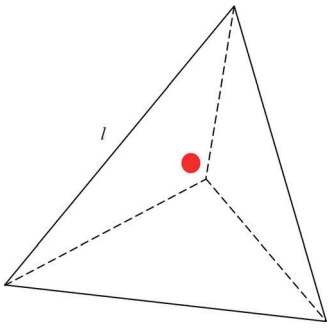

Figure 2. Tetrahedron element and SPH particle. *l* is the element edge length of the tetrahedron. The red dot is the SPH particle to be generated.

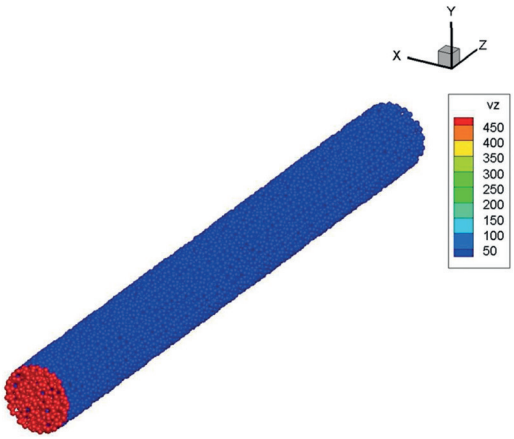

Figure 3. 3D model of ANFO. The diameter is 77 mm. LD ratio is10. The initial v_z of red particles is set to be 500 m s^{-1}.

The unreacted explosive is described by the Murnahan EoS with parameters $n=7.4$, $\kappa=3.9\times10^{-11}$ Pa^{-1} and $\rho_0=1160.0$ kg m^{-3}. The explosive products is described by modified JWL EoS with parameter $A=2.9867\times10^{11}$ Pa, $B=4.11706\times10^{9}$ Pa, $C=7.206147\times10^{8}$ Pa, $R_1=4.95$, $R_2=1.15$, $\omega=0.35$, and $\rho_0=1160.0$ kg m^{-3}. The reaction rate is described by an Equation of reaction rate with parameters $G=3.5083\times10^{-7}$ Pa^{-b}, Q is 0, $b=1.3$, and $\rho_0=1160.0$ kg m^{-3}.

4.1.1 Influence of Element Edge Length

As mentioned in the previous section, the particles of the 3D SPH models are generated through ANSYS. Element edge length, which is used to control the average edge length of tetrahedron element, is a fundamental parameter to determine the total number of ANFO models and furthermore, the accuracy of the SPH method.

According to Souers et al. [32], for JWL++ model, at least 4 zones per mm are required for the simulation of ANFO. However, similar research has not been done for the simulation of ANFO based on SPH method. Thus, in this section, the influence of element edge length on simulation has been investigated.

Series of length are used to investigate the influence of element edge length, as shown in Table 2.

In SPH method, smoothing length is a vital parameter which determines the influence domain of each particle, as described in the theoretical part in the previous section. Thus, it significantly influences the accuracy of SPH algorithm. An ill smoothing length can even cause failure of the method. Thus, a tuned smoothing length is necessitated

Table 2. Simulation to study the influence of the element edge length.

Element edge length [mm]	0.0109	0.0124	0.0140	0.0155	0.0171

for each simulation based on SPH method. Herein, a parameter called smoothing length coefficient is introduced, as shown in

$$L_{\text{initial smoothing length}} = l_{\text{element edge length}} \cdot \alpha \quad (42)$$

where L is the initial smoothing length (since smoothing length is updated at each time step, initial smoothing length is only used at the beginning), l is the element edge length, and α is the smoothing length coefficient.

The simulation result is presented in Figure 4, where the diameter is 77 mm, length-to-diameter ratio is 10, element edge length is 0.0109 mm, and smoothing length coefficient is 1.065.

As observed in Figure 4, the explosive product gradually expands as the detonation front propagates from left to right. The distribution of pressure, smoothing length and reaction progress at 400 μs is shown in Figure 5.

It can be clearly seen from Figure 6 that when element edge length is less or equivalent to 0.0140 mm, the simulation starts to stabilize and approach experiment. When element edge length is set to be 0.0155 mm, the simulation fluctuates obviously, especially in large-diameter simulation.

When the element edge length is further increased to 0.0171 mm, there is an abrupt decrease of detonation velocity at diameter 102 mm ($1/R$ is 0.01961 mm^{-1}), which severely deviates from experiment. Moreover, failure of implementation of the program is observed at diameter 153 mm, and that is why the simulation data is default at that point.

Furthermore, the simulation agrees better with experiment in large-diameter simulation ($R \geq 90$ mm). When diameter of ANFO cylinder is less than 90 mm, the simulation distinctly deviates from experiment, which may result from that fact that under the same element edge length, models

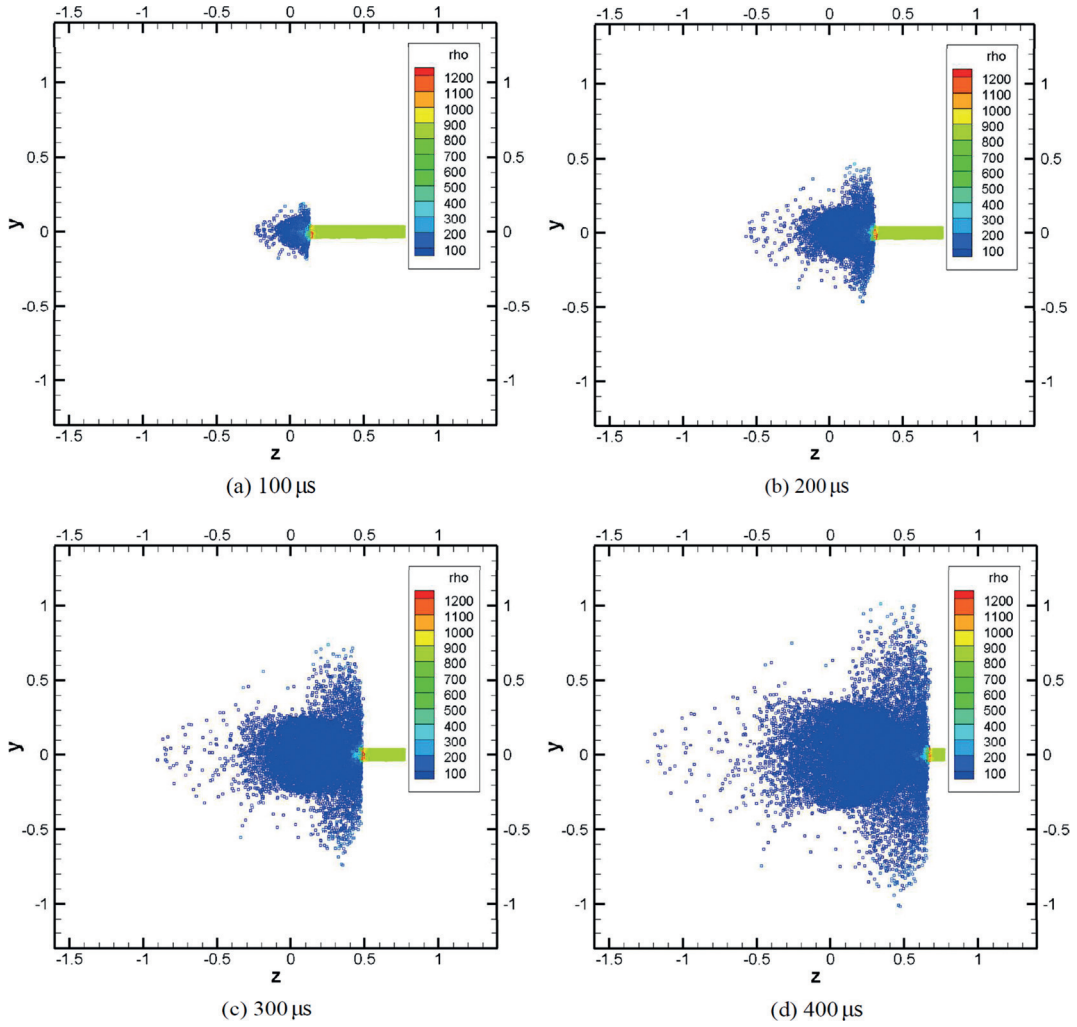

Figure 4. Expansion of detonated ANFO cylinders at different time steps: (a) 100 μs, (b) 200 μs, (c) 300 μs, (d) 400 μs.

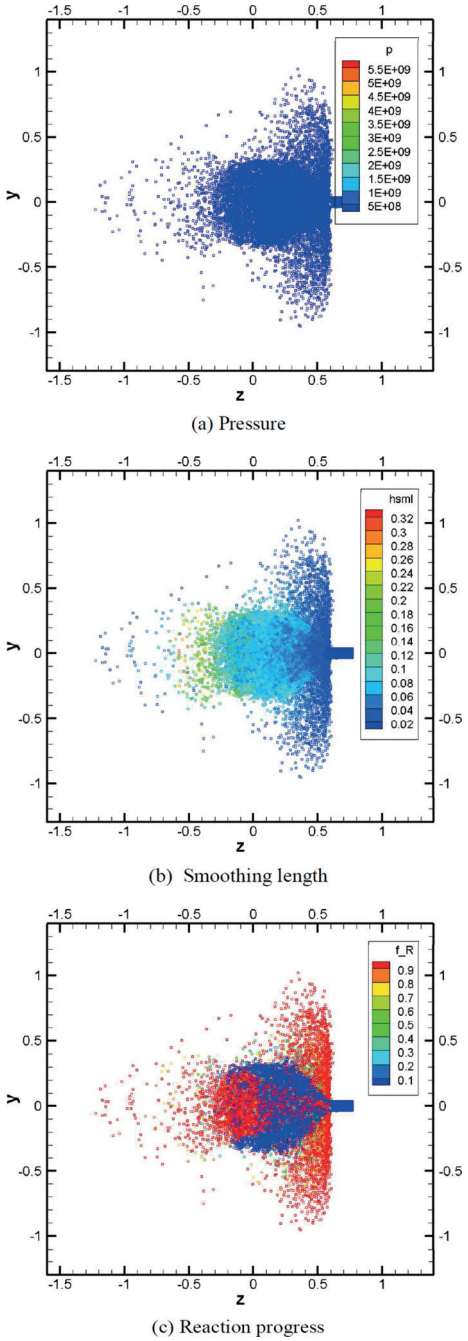

Figure 5. Distribution of pressure, smoothing length, and reaction progress at 400 µs. The influence of element edge length on simulation is shown in Figure 6. (a) Pressure. (b) Smoothing length. (c) Reaction progress.

with smaller diameter have much less particles, which reduces the accuracy of SPH method.

Thus, we can conclude from Figure 6 that the maximum element edge length to implement stable SPH simulation of ANFO is 0.0140 mm. The preferred element edge length is less or equivalent to 0.0124 mm. If element edge length is greater than 0.0171 mm, the algorithm will probably fail.

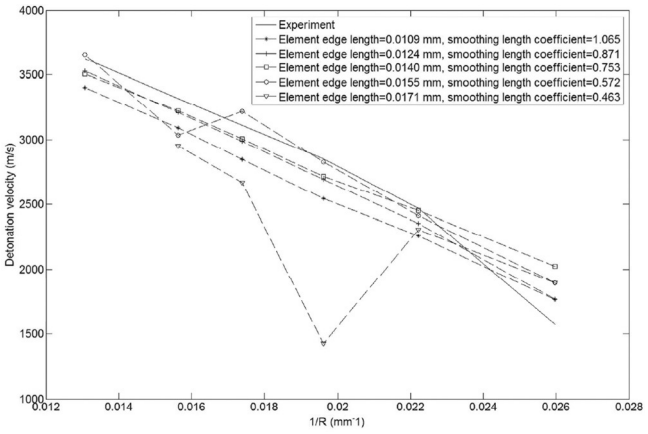

Figure 6. Influence of the element edge length.

4.1.2 Stability of the Simulation Result

During the simulation of ANFO, detonation velocity is calculated every 1000 time steps (one time step is 5×10^{-8} s). Thus, as the detonation front propagates from one end to the other end of the ANFO cylinder, detonation velocity will be calculated about 7–9 times. Thus, an average over the recorded detonation velocity from 3000th time step (Because recorded detonation velocity generally stabilizes from 2000th time step) is conducted to obtain an average detonation velocity, as is presented in the previous section. In this section, standard deviation is used to analyze the stability of average detonation velocity.

$$\sigma = \sqrt{\frac{1}{N-1}\sum_{i=1}^{N}(v_i - \bar{v})^2} \tag{43}$$

where v_i is the detonation velocity recorded each 1000 time steps, $\bar{v}$ is the average detonation velocity given by

$$\bar{v} = \frac{1}{N}\sum_{i=1}^{N} v_i \tag{44}$$

The result in presented in Figure 7, where the *x* axis represents diameter-to-element-edge-length ratio and the *y* axis represents standard deviation calculated for detonation velocity.

It can be seen from Figure 7 a–c that when the as diameter-to-element-edge-length ratio increases (means diameter of ANFO cylinder increases), the standard deviation of average detonation velocity tends to decrease, which means that under the same element edge length, the average detonation velocity tends to stabilize as the diameter of the cylinder increases.

For Figure 7 d and Figure 7 e, it can be seen that under these element edge length, standard deviation fluctuates violently, which indicates the SPH algorithm starts to become unstable.

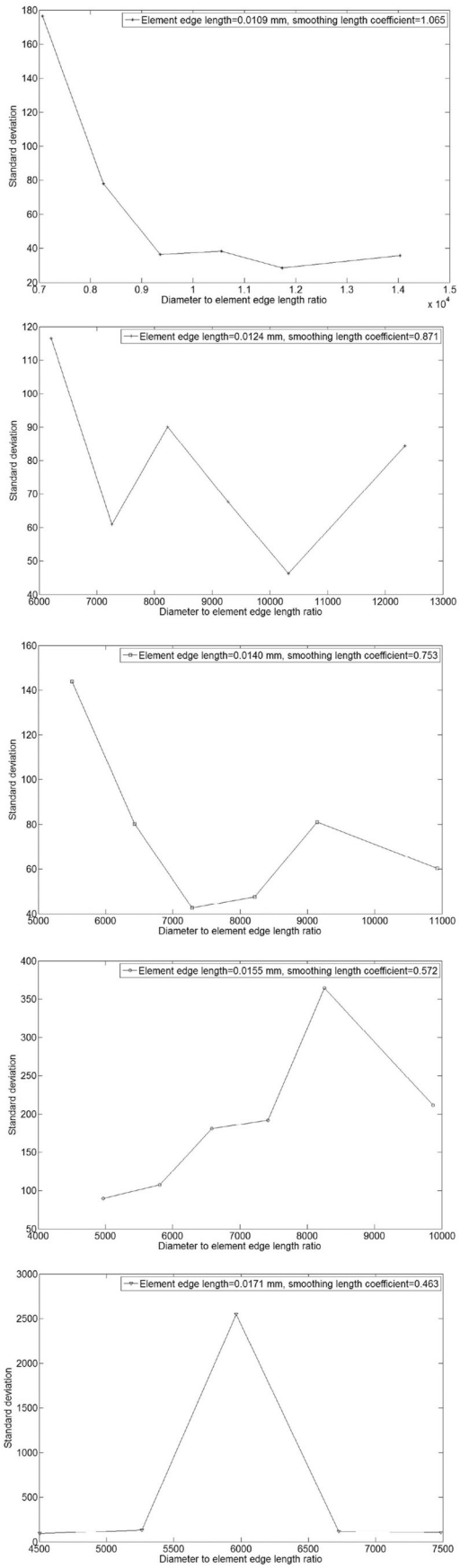

Figure 7. Influence of the element edge length on stability of ANFO model. (a) Standard deviation of average detonation velocity for element edge length 0.0109 mm. (b) Standard deviation of average detonation velocity for element edge length 0.0124 mm. (c) Standard deviation of average detonation velocity for element edge length 0.0140 mm. (d) Standard deviation of average detonation velocity for element edge length 0.0155 mm. (e) Standard deviation of average detonation velocity for element edge length 0.0171 mm.

4.1.3 Influence of Smoothing Length on Simulation

In SPH method, smoothing length is a vital parameter to determine the accuracy and performance of the algorithm. To investigate the influence of smoothing length, two smoothing length is applied for each simulation, as shown in Table 3.

Table 3. Simulation to study the influence of the smoothing length coefficient.

Element edge length [mm]	0.0109	0.0124	0.0140	0.0155	0.0171
Smoothing length coefficient α	1.18	0.968	0.837	0.636	0.514
	1.065	0.871	0.753	0.572	0.463

The simulation result is illustrated in Figure 8, where the *x* axis represents reverse of radius of ANFO cylinder and the *y* axis represents detonation velocity.

According to Figure 8 a, b, c, when the smoothing length coefficient increases, the detonation velocity decreases. For Figure 8 d and e, since the algorithm starts to become unstable, the influence of smoothing length coefficient on average detonation velocity is not clearly observed.

The influence of smoothing length coefficient on detonation velocity is shown in Table 4.

5 Conclusions

An improved SPH method incorporated with JWL++ model for 3D simulation of non-ideal ANFO is proposed. An innovative numerical technique, kernel gradient correction (KGC) method, is also applied to improve computational accuracy of the algorithm.

To validate the model, series of ANFO cylinders with diameters ranging from 77 mm to 153 mm are detonated. The detonation velocity is obtained and compared with experiment. The influence of element edge length on simulation was investigated and it is found that when element edge length is less or equivalent to 0.0140 mm, the SPH model starts to stabilize and approach experiment. Otherwise, the SPH will fluctuate and become unstable. The agreement between simulation and experiment is better for ANFO cylinders with larger diameter. We concluded that

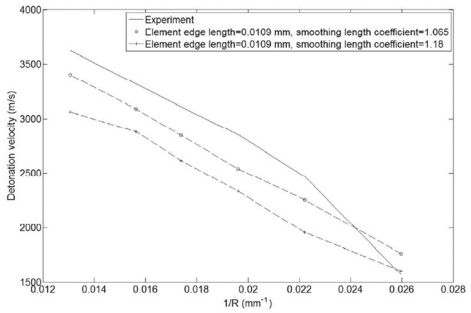

(a) Element edge length 0.0109 mm

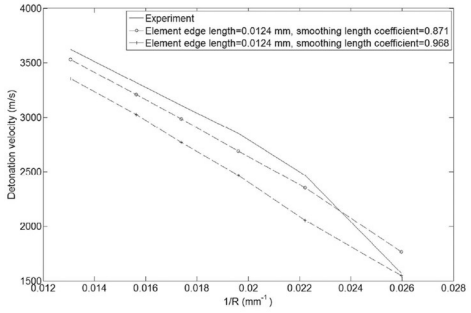

(b) Element edge length 0.0124 mm

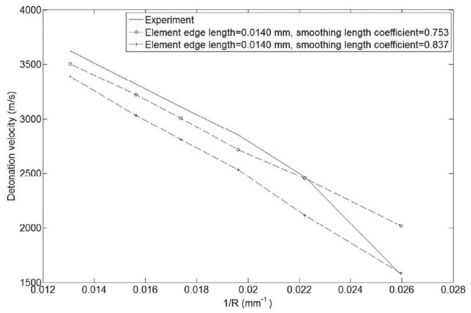

(c) Element edge length 0.0140 mm

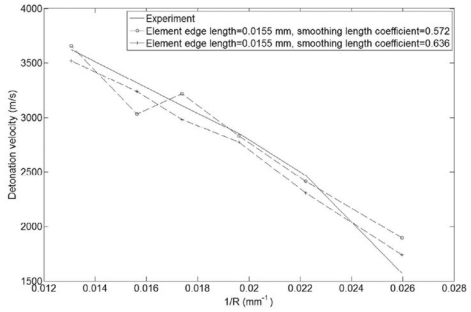

(d) Element edge length 0.0155 mm

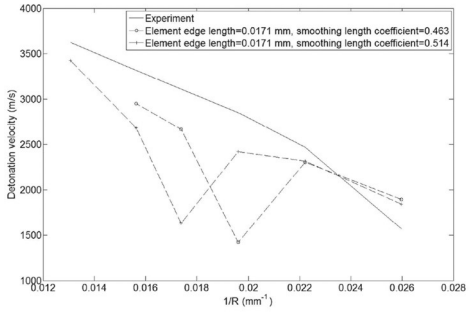

(e) Element edge length 0.0171 mm

Table 4. Influence of smoothing length coefficient on average detonation velocity.

		Diameter [mm]					
		77	90	102	115	128	153
Element edge length [mm]							
0.0109	1.18	1605.5	1955.9	2335.1	2616.5	2879.6	3063
	1.065	1764.5	2256.8	2541.9	2847.5	3088.7	3400.8
0.0124	0.968	1549.5	2057.6	2466.9	2770.3	3026.4	3354.5
	0.871	1768.8	2353.3	2690.2	2984.8	3208.8	3529.6
0.0140	0.837	1585.2	2115.7	2534.2	2809.2	3031.9	3388.5
	0.753	2020.9	2453.0	2716.0	3007.1	3220.6	3505.1
0.0155	0.636	1739.6	2308.8	2774.7	2983.8	3237.7	3521.5
	0.572	1896.4	2413.9	2828.6	3216.5	3032.8	3655.4
0.0171	0.514	1844.0	2315.0	2422.2	1632.9	2682.8	3425.9
	0.463	1894.9	2306.1	1424.6	2668.9	2950.2	default
Experimental detonation velocity [m s^{-1}]		1570.5	2468.0	2852.6	3109.0	3317.3	3621.8

the proposed SPH model is sufficiently accurate and reliable to study the detonation of non-ideal high-explosive ANFO.

Acknowledgments

The work is mainly supported by the United States DoD (DTRA): Grant # HDTRA1-13-1-0025.The Ohio Supercomputer Center is gratefully acknowledged for providing the computation source.

References

[1] M. Short, T. R. Salyer, T. D. Aslam, C. B. Kiyanda, J. S. Morris, T. Zimmerly, Detonation Shock Dynamics Calibration for Nonideal HE:ANFO, *AIP Conf. Proc.* **2009**, *1195*, 189–192.

[2] S. I. Jackson, C. B. Kiyanda, Experimental Observations of Detoantion in Ammonium-Nitrate-Fueloil (ANFO) Surrounded by a High-Sound-Speed, Shockless, Aluminum Confiner, *Proc. Combust. Inst.* **2011**, *33*, 2219–2226.

[3] J. B. Bdzil, T. D. Catanach, R. A. Hill, M. Short, R. A. Catanach, L. G. Hill, DSD Front Models: Non-Ideal Explosive Detonation in ANFO, *12th Symposium (International) on Detonation*, San Diego, CA, USA, August 11–16, **2002**.

[4] L. L. Davis, L. G. Hill, *ANFO Cylinder Test*, **2002**, 620, 165–168.

[5] J. B. Bdzil, T. D. Aslam, R. A. Catanach, DSD Front Models: Non-ideal Explosive Detonation in ANFO, *12th Symposium (International) on Detonation*, San Diego, CA, USA, August 11–16, **2002**.

[6] R. A. Borg, D. A. Jones, *Numerical Simulation of Projectile Impact Experiments Using the Forest Fire Reaction Rate Model*, DSTO Publications, Canberra **1996**.

Figure 8. Influence of smoothing length coefficient on the average detonation velocity. (a) Element edge length 0.0109 mm. (b) Element edge length 0.0124 mm. (c) Element edge length 0.0140 mm. (d) Element edge length 0.0155 mm. (e) Element edge length 0.0171 mm.

[7] A. K. Kapila, D. W. Schwendeman, J. B. Bdzil, W. D. Henshaw, A Study of Detonation Diffraction in the Ignition-and-Growth Model, *Combust. Theor. Model.* **2007**, *11*, 781 – 822.
[8] A. K. Kapila, D. W. Schwendeman. Numerical Studies of Detonation Diffraction Using the Ignition-and-Growth Model. *20th International Colloquium on Dynamics of Explosions and Reactive Systems*, Montreal, Canada, October 20–22, **2005**.
[9] P. C. Souers, S. Anderson, J. Mercer, E. McGuire, P. Vitello, JWL + +: A Simple Reactive Flow Code Package for Detonation, *Propellants Explos. Pyrotech.* **2000**, *25*, 54–58.
[10] C. M. Tarver, E. M. McGuire, Reactive Flow Modeling of the Interaction of TATB Detonation Waves with Inert Materials, *12th Symposium (International) on Detonation*, San Diego, CA, USA, August 11–16, **2002**.
[11] M. L. Garcia, C. M. Tarver, Three Dimensional Ignition and Growth Reactive Flow Modeling of Prism Faliure Tests on PBX 9502, *13th Symposium (International) on Detonation*, Norfolk, VA, USA, July 23–28, **2006**.
[12] J. E. Guilkey, T. B. Harman, B. Banerjee, An Eulerian-Lagrangian Approach for Simulating Explosions of Energetic Devices, *Comput. Struct.* **2007**, *85*, 660 – 674.
[13] K. H. Kim, J. J. Yoh, A Particle Level-Set Based Eulerian Method for Multi-material Detonation Simualtion of High Explosive and Metal Confinements, *Proc. Combust. Inst.* **2013**, *34*, 2025 – 2033.
[14] D. C. Sorescu, D. L. Thompson. Classical and Quantum Mechanical Studies of Crystalline Ammonium Nitrate, *J. Phys. Chem. A* **2001**, *105*, 720 – 733.
[15] D. L. Robbins, S. A. Sheffield, D M Dattelbaum, N. Velisavljevic, D. B. Stahl, Equation of State of Ammonium Nitrate, *Shock Compress. Condens. Matter* **2009**, *1195*, 552 – 555.
[16] R. S. Chellappa, D. M. Dattelbaum, N. Velisavljevic, S. Sheffield, The Phase Diagram of Ammonium Nitrate, *J. Chem. Phys.* **2012**, *137*, 064504.
[17] R. A. Gingold, J. J. Monaghan, Smoothed Particle Hydrodynamics – Theory and Application to Non-Spherical Stars, *Mon. Not. R. Astron. Soc.* **1977**, *181*, 375 – 389.
[18] L. B. Lucy, A Numerical Approach to the Testing of the Fission Hypothesis, *Astronomical J.* **1977**, *82*, 1013 – 1024.
[19] G. R. Liu, M. B. Liu, *Smoothed Particle Hydrodynamics: A Meshfree Particle Method*, World Scientific, Singapore, **2003**.
[20] M. B. Liu, G. R. Liu, Z. Zong, K. Y. Lam, Computer Simulation of High Explosive Explosion Using Smoothed Particle Hydrodynamics Methodology, *Computer Fluids* **2003**, *32*, 305 – 322.
[21] M. B. Liu, G. R. Liu, K. Y. Lam, Z. Zong, Smoothed Particle Hydrodynamics for Numerical Simulation of Underwater Explosion, *Comput. Mechanics* **2003**, *30*, 106 – 118.
[22] M. B. Liu, G. R. Liu, K. Y. Lam, Z. Zong, Meshfree Particle Simulation of the Detonation Process for High Explosives in Shaped Charge Unlined Cavity Configurations, *Shock Waves* **2003**, *12*, 509 – 520.
[23] D. Feng, M. B. Liu, H. Li, G. R. Liu, Smoothed Particle Hydrodynamics Modeling of Linear Shaped Charge with Jet Formation and Penetration Effects, *Computers Fluids* **2013**, *86*, 77 – 85.
[24] J. J. Monaghan, R. A. Gingold, Shock Simualtion by the Particle Method SPH, *J. Comput. Phys.* **1983**, *52*, 374 – 389.
[25] J. J. Monaghan, J. Poinracic, Artificial Viscosity for Particle Methods, *Appl. Numer. Math.* **1985**, *1*, 187 – 194.
[26] J. J. Monaghan, SPH Meets the Shocks of Noh, Monash University, Monash, Western Australia, **1987**.
[27] J. R. Shao, H. Q. Li, G. R. Liu, M. B. Liu, An Improved SPH Method for Modeling Liquid Sloshing Dynamics, *Comput. Struct.* **2012**, *100–101*, 18 – 26.
[28] W. Benz, Smooth Particle Hydrodynamics: A Review, *NATO ASI Ser.* **1990**, *302*, 269–288.
[29] E. L. Lee, H. C. Hornig, J. W. Kury, *Adiabatic Expansion of High Explosive Detonation Products*, University of California Livermore, Lawrence Livermore Radiation Laboratory, Livermore, CA, USA, **1968**.
[30] J. W. Kury, H. C. Hornig, E. L. Lee, Metal Acceleration by Chemical Explosives, *4th Symposium (International) on Detonation,* Silver Spring, MD, USA, October 12–15, **1965**, p. 3–13.
[31] E. L. Lee, H. C. Hornig, Equation of State of Detoantion Product Gases, *12th International Symposium on Combustion*, Poitiers, France, July 14–20, **1968**, p. 493–499.
[32] P. C. Souers, R. Garza, P. Vitello, Ignition and Growth and JWL + + Detonation Models in Coarse Zones, *Propellants Explos. Pyrotech.* **2002**, *27*, 62 – 71.

Received: October 12, 2014
Revised: November 21, 2014
Published online: January 30, 2015

